

Uncertainty in Acoustic Mine Detection Due to Environmental Variability

Dr. Peter C. Chu¹, LCDR Nick A. Vares¹, Ms. Ruth E. Keenan²

1) Naval Ocean Analysis and Prediction Laboratory, Naval Postgraduate School, Monterey CA 93943

2) Scientific Application International Corporation, Mashpee, MA02649

Abstract - Uncertainty in acoustic bottom target detection due to environmental variability for a shallow sea (30 m water depth) is investigated using the Navy's Comprehensive Acoustic Simulation System/Gaussian Ray Bundle model for a generic Very High Frequency (VHF) forward looking sonar. The effects of imprecise bottom type and wind speed data are evaluated to determine the impact of this variability on bottom target detection. The acoustic uncertainty due to the wind variability is more sensitive to muddy sand than to and sandy silt. Maximum acoustic uncertainty due to wind variability is 9 dB for the muddy sand and 6 dB for the sandy silt. For the bottom target detection, the wind speed accuracy is extremely important. If wind speed uncertainty exceeds 7 kts, the bottom target is unlikely to be detected. The signal excess variability is small and operational benefits may be maximized with slightly better sonar. Deep transducer (depth: 25 m) demonstrates substantial signal excesses up to 23 dB compared to 7 dB for shallow transducer (depth: 5.18 m). Therefore, to increase the probability of bottom target detection utilizing the generic VHF forward looking sonar, placement of the transducer deeper in the water column is recommended.

1. Introduction

The United States military has undergone numerous changes since the end of the Cold War. Specifically, the US Navy experienced a shift in the area of engagement from the "blue water" (water depth greater than 100 m) Soviet threat, to littoral regions of the world. Sensors, tactics and platforms optimized to perform in a deep ocean, acoustically range independent environment operate inadequately in shallow, acoustically range dependent littoral regions. Littoral regions are reverberation limited and more complicated than the deep ocean.

Most countries lack the robust Gross National Product of the US and have no intention of ever building a navy to oppose US Naval forces on the open seas in Mahanian fashion. The decision to focus naval military budgets on

economical and lethal alternatives is prudent, as countries retreat to coastal defense postures. The weapons of choice are diesel submarines and sea mines, both of which present a credible threat to invading forces and require a disproportionately larger neutralizing force.

Diesel submarines are very quiet, difficult to detect and a thrifty alternative to nuclear submarines. Technological advancements in battery design have resulted in higher capacity batteries with shorter recharge times. When employed for coastal defense, the long endurance advantage of nuclear submarines is negligible to these countries.

Mines come in a multitude of variations and are readily available on the international market. Mines are designed to operate throughout the water column; on the surface, at various depths and on the bottom (Fig. 1). There are an assortment of actuators including contact, magnetic influence and acoustic. The incorporation of counters, where the mine detonates after a set number of trigger signals, can mask the presence of a minefield.

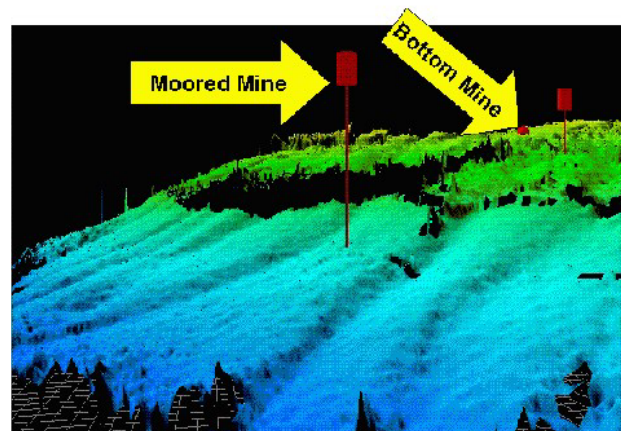


Fig.1. Mine placement in the water column (After CNO-N77, 2002).

In terms of cost effectiveness, mines are cheap to procure, deploy and require no upkeep once deployed. Any nation can acquire mass quantities of mines at far lower prices than shipbuilding. A single World War I Iranian contact mine in the Persian Gulf caused \$96 million worth of damage to the USS Samuel B. Roberts (FFG-58) in April 1988. The return on investment is enormous, a cheap mine does significant damage and possibly removes an enemy ship from the theater. Mine deployment is uncomplicated and can be performed from basic surface craft. As evidenced by the Samuel B. Roberts, mines have the potential for long life spans without maintenance. The low target strength of mines combined with the complex littoral environment hinders minesweeping efforts.

Active sonar and unique High Frequency (HF) sonar systems along with Unmanned Undersea Vehicles (UUVs) are the new means to counter diesel submarines and mines. Active sonar has long been viewed by the submarine force with apprehension, since it gives away own ships position at twice the range of detection. New tactics for employing active sonar against diesel submarines have served to relieve deep rooted reservations and resulted in greater detection ranges. HF sonar generates higher resolution images necessary to distinguish mine-like objects from actual mines (Fig. 2).



Fig. 2. HF active sonar array mounted in the sail of the USS Asheville, a 688i Los Angeles Class submarine (From N77, 2002).

UUVs are essential to extend the sensor range of naval platforms and evaluate minefields without jeopardizing military lives. Specialized sonar systems, improved maneuverability and faster minefield assessment with the use of multiple UUVs make this a valuable asset to the Navy (Fig. 3).

The Navy's standard model for range dependent acoustic propagation, the Comprehensive Acoustic Simulation System (CASS) incorporates the Gaussian Ray Bundle (GRAB) eigenray model, in the 600 Hz to 100 kHz

frequency band (Keenan, 2000). This reverberation model works well to predict acoustic performance in the littorals for signal excess given accurate inputs, such as bottom type, sound speed profile and wind speed. In 1980 the Generic Sonar Model evolved into CASS, consisting of system, acoustic and sonar analysis models (Weinberg, 2000).

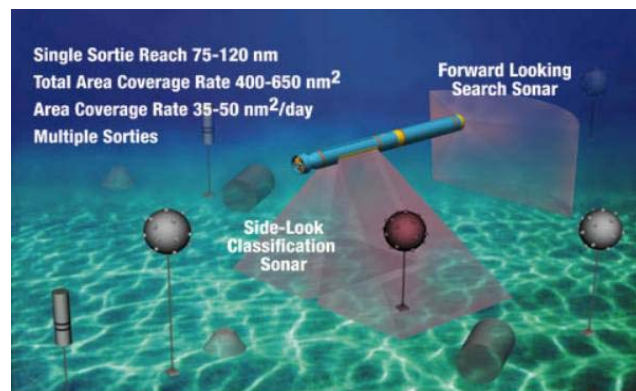


Fig. 3. UUV sonar systems and capabilities (From CNO-N77, 2002).

Very high frequency (VHF) sonar systems are popularly used to generate high-resolution images for acoustic target detection. Sensors, tactics and platforms optimized to perform in a deep ocean, acoustically range independent environment operate inadequately in shallow, acoustically range dependent littoral regions. Littoral regions are reverberation limited and more complicated than the deep ocean.

Recently, a generic sonar model evolved into the Navy's Comprehensive Acoustic Simulation System (CASS) for acoustic and sonar analysis (Weinberg, 2000). It incorporates the Gaussian Ray Bundle (GRAB) eigenray modes to predict the monostatic and bistatic range dependent acoustic propagation for 600 Hz to 100 kHz frequency band (Keenan, 2000, Chu et al., 2002, 2003). Test rays are sorted into families of comparable numbers of turning points and boundary interactions. Ray properties are then power averaged for each ray family to produce a representative eigenray of that family. The signal excess (SE) is computed by summing all eigenray path combinations for a range bin, and then the peak signal is used to determine the reverb/noise level.

CASS/GRAB simulates the sonar performance reasonably well in the littoral zone with given accurate environmental input data, such as bottom type, sound speed profile and wind speed and accurate tilt angle of the sound source (Weinberg and Keenan, 1996). However, the environmental data are usually inaccurate. The effect of environmental variability on the acoustic propagation uncertainty should be investigated.

Recently, Chu et al. (2002) investigated the acoustic uncertainty in the Yellow Sea continental shelf due to sound speed profile uncertainty using CASS/GRAB and found that the level of acoustic uncertainty depends on location of sound speed profile errors relative to the sound source. When a Gaussian-type noise is introduced into the sound speed profiles, the detection range anomaly has non-Gaussian-type distribution in winter and Gaussian-type distribution in summer, and is much larger in winter than in summer for the same noise intensity. In winter, when an error (+1 m/s) is added into the sound speed profile at the source depth, a shadow zone is formed in front of the source that significantly decreases the detection ranges at that depth. When an error (-1 m/s) is added into the sound speed profile at the source depth, a strong sound channel formed that dramatically increases the detection ranges at that depth. In their study, the surface winds and the bottom type are assumed accurate.

The surface wind data over the ocean are highly uncertain (Chu et al. 1998), and so as the bottom type data. Many parts of the world have inadequate bottom type mapping in littoral regions and covert reconnaissance may be the only source of approximate bottom information. Bottom types can vary greatly in a small area and effect actual acoustic performance as bottom interaction changes.

What is the effect of surface wind and bottom type variability on the acoustic uncertainty? and in turn what is the effect on a generic VHF forward looking sonar's performance?

2. CASS/GRAB Model

2.1. Ray Tracing

Let (x, y) and z are the horizontal and vertical coordinates and r be the horizontal range. Let (P, P_0) be the acoustic pressure at (x, y, z) and at a reference distance (r_0) from the source (Fig. 4). The horizontal and vertical slowness for the ν -th ray is represented by

$$p_{r,\nu} = \frac{\cos \theta_\nu}{c_\nu}, \quad p_{z,\nu} = \frac{\sin \theta_\nu}{c_\nu} \quad (10)$$

where c_ν is the sound speed, and θ_ν the horizontal inclination angle. The travel time $(T_{z,\nu})$ at the field-point depth z is computed from T_ν by

$$T_{z,\nu} = T_\nu + p_{z,\nu} (z - z_\nu). \quad (11)$$

Volume attenuation and boundary reflection losses are represented by the pressure ratio Γ_ν and phase shift Φ_ν , respectively. Rayleigh bottom "forward" loss is determined

from the first three columns of the geo-acoustic table for various bottom types (Table 1). Duplicate grain size indexes are listed to cover all commonly used geo-acoustic bottom types. Six geo-acoustic parameters are used to calculate

$$\Gamma_\nu = \Pi \gamma_{s,\nu} \times \Pi \gamma_{b,\nu}, \quad \Phi_\nu = \sum \phi_{s,\nu} + \sum \phi_{b,\nu} \quad (13)$$

where $\gamma_{s,\nu}$ is the surface reflection coefficient amplitude; $\gamma_{b,\nu}$ is the bottom reflection coefficient amplitude; $\phi_{s,\nu}$ and $\phi_{b,\nu}$ are the surface and bottom phase shifts.

Bottom Composition	Grain Size	Long Name	Density	Sound Speed Ratio	Wave Number Ratio	Volume Parameter ***	Spectral Exponent ***	Spectral Parameter ***
BOULDER	-9.0	ROUGH ROCK	2.500	2.5000	0.01374	0.0020	3.25	0.206930
ROCK	-7.0	ROCK	2.500	2.5000	0.01374	0.0020	3.25	0.018620
	-3.0	COBBLE	2.500	1.8000	0.01374	0.0020	3.25	0.016000
GRAVEL	-3.0	GRAVEL	2.500	1.8000	0.01374	0.0020	3.25	0.016000
	-3.0	PEBBLE	2.500	1.8000	0.01374	0.0020	3.25	0.016000
	-1.0	SANDY GRAVEL	2.492	1.3370	0.01705	0.0020	3.25	0.012937
	-0.5	VERY COARSE SAND	2.401	1.3067	0.01667	0.0020	3.25	0.010573
	0.0	MUDDY SANDY GRAVEL	2.314	1.2778	0.01630	0.0020	3.25	0.008602
	0.5	COARSE SAND	2.231	1.2503	0.01638	0.0020	3.25	0.006957
	0.5	GRAVELLY SAND	2.231	1.2503	0.01638	0.0020	3.25	0.006957
	1.0	GRAVELLY MUDDY SAND	2.151	1.2241	0.01645	0.0020	3.25	0.005587
SAND	1.5	SAND	1.845	1.1782	0.01624	0.0020	3.25	0.004446
	1.5	MEDIUM SAND	1.845	1.1782	0.01624	0.0020	3.25	0.004446
	2.0	MUDDY GRAVEL	1.615	1.1396	0.01610	0.0020	3.25	0.003496
	2.5	FINE SAND	1.451	1.1073	0.01602	0.0020	3.25	0.002715
	2.5	SILTY SAND	1.451	1.1073	0.01602	0.0020	3.25	0.002715
	3.0	MUDDY SAND	1.339	1.0800	0.01728	0.0020	3.25	0.002070
	3.5	VERY FINE SAND	1.288	1.0588	0.01875	0.0020	3.25	0.001544
	4.0	CLAYEY SAND	1.224	1.0384	0.02019	0.0020	3.25	0.001119
	4.5	COARSE SILT	1.195	1.0179	0.02158	0.0020	3.25	0.000781
	5.0	SANDY SILT	1.169	0.9999	0.01261	0.0020	3.25	0.000518
	5.5	MEDIUM SILT	1.149	0.9885	0.00675	0.0010	3.25	0.000518
	5.5	SAND-SILT-CLAY	1.149	0.9885	0.00675	0.0010	3.25	0.000518
SILT	6.0	SILT	1.149	0.9873	0.00386	0.0010	3.25	0.000518
	6.0	SANDY MUD	1.149	0.9873	0.00386	0.0010	3.25	0.000518
	6.5	FINE SILT	1.148	0.9861	0.00306	0.0010	3.25	0.000518
	6.5	CLAYEY SILT	1.148	0.9861	0.00306	0.0010	3.25	0.000518
MUD	7.0	SANDY CLAY	1.147	0.9849	0.00242	0.0010	3.25	0.000518
	7.5	VERY FINE SILT	1.147	0.9837	0.00194	0.0010	3.25	0.000518
	8.0	SILTY CLAY	1.146	0.9824	0.00163	0.0010	3.25	0.000518
CLAY	9.0	CLAY	1.145	0.9800	0.00148	0.0010	3.25	0.000518
	10.0		1.145	0.9800	0.00148	0.0010	3.25	0.000518

Table 1. Bottom type geo-acoustic properties (From NAVO, 1999).

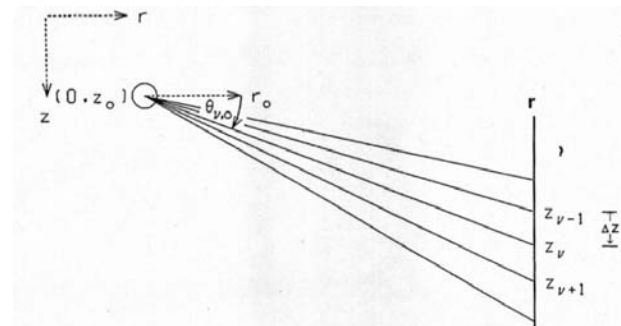


Fig. 4. Fan of acoustic rays.

2.2. Gaussian Ray Bundles

The energy conservation for simple geometric acoustics states that energy in a ray tube is equivalent to the energy in the ray tube at a reference range (Fig. 5). Different from the classical ray theory, the Gaussian ray bundle amplitudes of

the ν -th test ray at target depth z (Ψ_ν) is computed by (Weinberg and Keenan, 1996)

$$\Psi_\nu = \frac{\beta_{\nu,0} \Gamma_\nu^2}{\sqrt{2\pi} \sigma_\nu p_{r,\nu} r} \exp \left\{ -0.5 \left[\frac{z - z_\nu}{\sigma_\nu} \right]^2 \right\},$$

where σ_ν is the standard deviation and $\beta_{\nu,0}$ is the source-dependent conversion term to equate energy within a Gaussian ray bundle with a geometric-acoustic ray tube,

$$\beta_{\nu,0} = r_0^2 p_{r,\nu,0} \Delta\theta_{\nu,0} P_0^2. \quad (14)$$

Summation of the Gaussian ray bundle amplitudes over all the rays,

$$\Psi_e = \sum_\nu \Psi_\nu,$$

is the Gaussian eigenray and its square root, $A_e = \sqrt{\Psi_e}$, is defined as the Gaussian eigenray amplitude (A_e). The ratio Ψ_ν / Ψ_e , represents the weight of the ν -th ray. The acoustic characteristics are the weighted averages of the ray bundle properties such as the source angle, horizontal slowness, vertical slowness, boundary phase shift, and travel time,

$$\begin{aligned} \theta_e &= \Psi_e^{-1} \sum_\nu \Psi_\nu \theta_{\nu,0}, \\ p_{r,e} &= \Psi_e^{-1} \sum_\nu \Psi_\nu p_{r,\nu}, \quad p_{z,e} = \Psi_e^{-1} \sum_\nu \Psi_\nu p_{z,\nu}, \\ \Phi_e &= \Psi_e^{-1} \sum_\nu \Psi_\nu \Phi_\nu, \quad T_e = \Psi_e^{-1} \sum_\nu \Psi_\nu T_{z,\nu}. \end{aligned} \quad (23)$$

From these representative eigenrays, coherent or random propagation loss is calculated.

GRAB contains sound speed conversion models such as Leroy's equation (Leroy, 1969) and Millero-Li's equation (Millero, 1994), which is an adjustment to the original Chen-Millero equation (Chen, 1977). The Wilson's equation for temperature-salinity-sound speed conversion (Wilson, 1960) is used. GRAB defaults to Leroy's equation for sound speed conversions, where numerically stable polynomials are fit to Wilson's data.

3. Acoustic Uncertainty due to Bottom Type Variability

Let the transducer be placed at 5.18 m (17 ft) with a downward tilt angle of 4° in a shelf sea (water depth of 30 m) with a constant wind forcing (5 m/s). The characteristics of the acoustic detection are identified at the sea bottom with range varying from 0 to 1200 m.

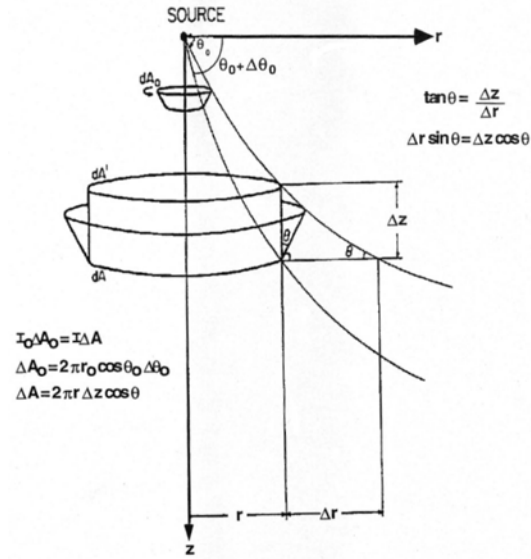


Fig. 5. Acoustic ray bundle.

3.1. Variability around Muddy Sand

The grain size index for the muddy sand is 3.0 (Table 1). The bottom type varies from muddy gravel to clayey sand that is represented by the grain size index varying between 2.0 (for muddy gravel) and 4.0 (for clay sand) with 0.5 increments. The simulated signal at the sea bottom varies drastically (60-82 dB) for the range less than 100 m, increases to a peak of 90 dB at range around 130 m, and then decreases to 38 dB at range of 1200 m (Fig. 6a). The signal variability due to the change of the grain size index is 2 dB at the peak (range around 130 m), and reduces to less than or equal to 1 dB as the range increases to 1200 m.

The simulated reverberation at the sea bottom varies drastically with range with a peak of 90 dB at range about 130 m, and reduces to roughly 47 dB at 1200 m (Fig. 6b). Greater uncertainty due to the grain size variability is found in the reverberation than in the signal. The reverberation uncertainty is small (1 dB) for range smaller than 100 m, increases to 3 dB at range of 130 m (peak reverberation), reduces to 1 dB again at range of 250 m, and increases to 4 dB at range of 1200 m.

The signal excess at the bottom varies with range rapidly (20 dB) for ranges from 0 to 100 m, increases with range to a peak of 4 dB at range of 200 m, then decreases with range to -14 dB at range of 1200 m (Fig. 6c). The variability of signal excess due to bottom type variability is about 3.5 dB at the peak (at the range of 200 m), decreases slightly to 3 dB from range of 200 m to 800 m, and then decreases to 1 dB at range of 1200 m. The histogram of CASS/GRAB simulated signal excess at the sea bottom for muddy sand variability (Fig. 7) shows negatively skewed with majority values lying between -5 dB and -7 dB.

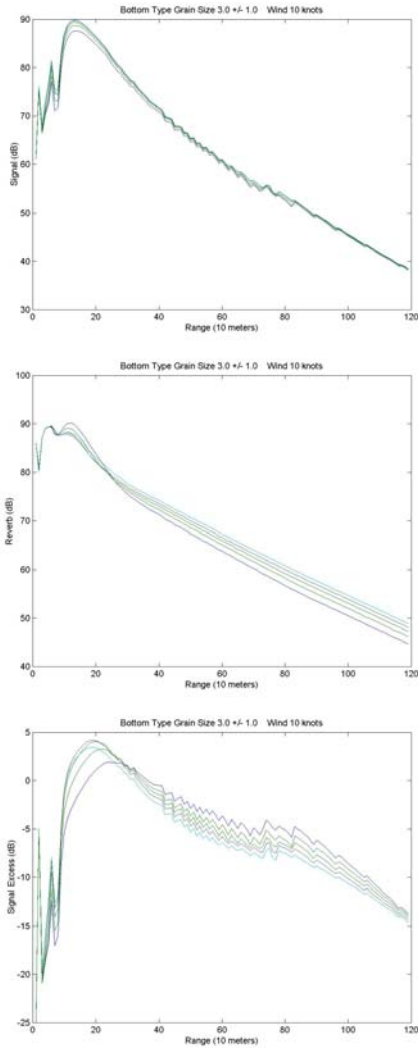


Fig. 6. Range dependent effect of muddy sand variability on mine acoustic detection at the sea bottom simulated using CASS/GRAB with surface wind speed of 5 m/s: (a) signal, (b) reverberation, and (c) signal excess.

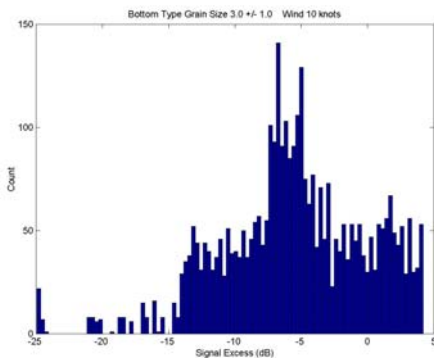


Fig. 7. Histogram of CASS/GRAB simulated signal excess with surface wind speed of 5 m/s at the sea bottom for muddy sand variability.

3.2. Variability around Sand Silt

The grain size index for the sand silt is 5.0 (Table 1). The bottom type varies from clayey sand to sand silt that is represented by the grain size index varying between 4.0 (for clay sand) and 6.0 (for silt) with 0.5 increments. The simulated signal at the sea bottom varies drastically (60-75 dB) for the range smaller than 100 m, increases to a peak of 88 dB at range around 130 m, and then decreases to 38 dB at range of 1200 m (Fig. 8a). The signal variability due to the change of the grain size index is 3 dB at the peak (range around 130 m), and increases to 4 dB at range of 700 m and then decreases to 2 dB at range of 1200 m.

The simulated reverberation at the sea bottom varies drastically with range with a peak of 91 dB at range about 130 m, and reduces to roughly 43 dB at 1200 m (Fig. 8b). The same as the muddy sand, greater uncertainty due to the grain size variability is found in the reverberation than in the signal. The reverberation uncertainty is small (less than 1 dB) for range smaller than 100 m, increases to 3 dB at range of 130 m (peak reverberation), and continue to increase to 6 dB at range of 1200 m.

The signal excess at the bottom varies with range rapidly (18 dB) for ranges from 0 to 100 m, increases with range to a peak of 2 dB at range of 250 m, then decreases with range to -14 dB at 1200 m (Fig. 8c). The variability of signal excess due to bottom type variability is about 6 dB at the peak (at the range of 250 m), decreases slightly to 5 dB from range of 250 m to 750 m, and then decreases to 1.5 dB at range of 1200 m. The histogram of CASS/GRAB simulated signal excess at the sea bottom for muddy sand variability (Fig. 4) shows negatively skewed with majority values lying between -1 dB and -4 dB. The signal excess has less standard deviation for sand silt variability (Fig. 9) than for muddy sand variability (Fig. 7). This indicates that the muddy sand variability causes more acoustic uncertainty in signal excess over range than the sand silt variability.

4. Acoustic Uncertainty due to Surface Wind Variability

Let the transducer be placed at 5.18 m (17 ft) with a downward tilt angle of 4° in a shelf sea (water depth of 30 m). The range for identifying the acoustic detection at the sea bottom is up to 1200 m. Two bottom types, muddy sand (index: 3.0) and sandy silt (index: 5.0), are used. The wind variability is taken as 2.5 m/s to 7.5 m/s.

4.1. Muddy Sand

The simulated signal at the sea bottom varies drastically (60-82 dB) for the range less than 50 m, increases to a peak

of 89 dB at range around 130 m, and then decreases to 37-42 dB at range of 1200 m (Fig. 10a). The signal variability due to the change of the wind is negligible for range less than 450 m, and then increases with range to 5 dB at range of 1200 m.

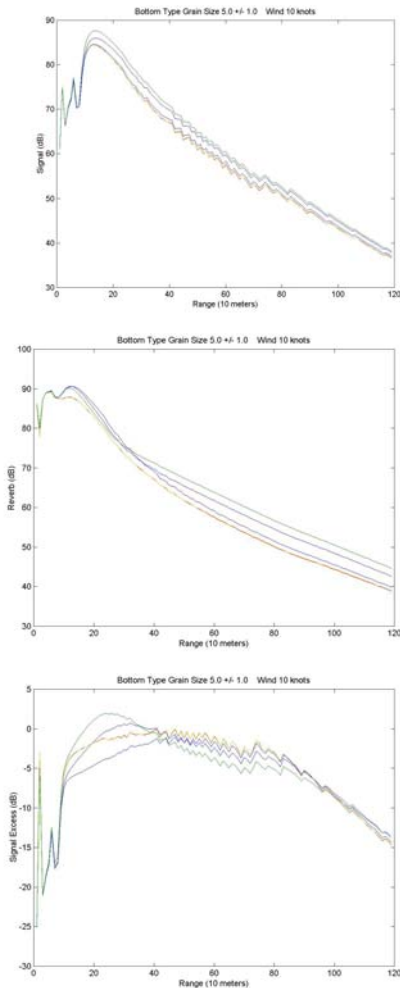


Fig.8. Range dependent effect of sand silt variability on acoustic detection at the sea bottom simulated using CASS/GRAB with surface wind speed of 5 m/s: (a) signal, (b) reverberation, and (c) signal excess.

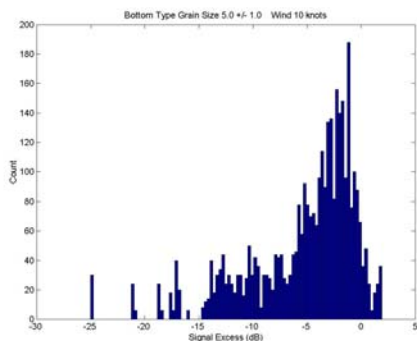


Fig. 9. Histogram of CASS/GRAB simulated signal excess with surface wind speed of 5 m/s at the sea bottom for sand silt variability.

Greater uncertainty due to the wind speed variability is found in the reverberation than in the signal. The reverberation uncertainty is 16 dB (82-98 dB) for range less than 50 m, reduces with the range from 16 dB at 50 m to 4 dB at 130 m, increases with the range to 9 dB at 330 m, and then slowly reduces to 4 dB at 1200 m (Fig. 10b).

Signal excess oscillates as range less than 100 m, peaking at 6 dB as range around 200 m, and then decays to -13 dB at range of 1200 m. The signal excess variability is relatively large, being 4.5 dB at range of 200 m, increasing to a maximum value about 9 dB from 320 m to 800 m, and then decreasing to 6 dB at 1200 m (Fig. 10c). Since the surface wind variability is 5 m/s. The maximum uncertainty of the signal excess caused by wind variability can be roughly estimated as 2 dB per 1 m/s wind variation. The histogram of simulated signal excess at the sea bottom for muddy sand with surface wind variability shows negatively skewed with majority values lying between -2 dB and -11 dB (Fig. 11).

4.2. Sand Silt

The simulated signal at the sea bottom varies between 65 dB and 75 dB for the range smaller than 100 m, increases to a peak of 85 dB at range around 130 m, and then decreases to 35 - 40 dB at range of 1200 m (Fig. 12a). The signal is not affected by the wind variability for range less than 700 m. The signal variability due to the change of the surface wind is almost zero for range less than 700 m and enhances with range to 5 dB at range of 1200 m.

Greater uncertainty due to the wind speed variability is found in the reverberation than in the signal. The reverberation uncertainty is 14 dB (82-96 dB) for range less than 50 m, reduces with range to near 0 dB at range of 130 m, and keeps 0 dB until range of 300 m, and then increases with the range to 8 dB at 1200 m (Fig. 12b).

Signal excess oscillates as range less than 100 m, peaking at 2 dB as range around 750 m, and then decays to -14 dB (-12 dB to -16 dB) at range of 1200 m. The signal excess variability is smaller for sand silt than for clay sand, vanishes at range of 230 m, increases to a maximum value of 6 dB at range of 750 m (peak reverberation value), followed by slowly decreases to 5 dB at 1200 m (Fig. 12c). Since the surface wind variability is 5 m/s. The maximum uncertainty of the signal excess caused by wind variability can be roughly estimated as 1 dB per 1 m/s wind variation. The histogram of simulated signal excess at the sea bottom for muddy sand with surface wind variability shows negatively skewed with majority values lying between -1 dB and -6 dB (Fig. 13).

The effects of wind speed variation for sandy silt are less than that of muddy sand, with a peak variation of 6 dB over a short distance and 5 dB variations for less than half the range (i.e., 600 m). Sonar equipment with an improved gain of 1 to 6 dB would significantly enhance detection range by widening the window of detection. The variations for sandy silt are most significant closer than 100 m and greater than 750 m, for ranges that lie outside of this, variations are less than 5 dB. Wind speed accuracy is therefore more important to accurate acoustic modeling for muddy sand.

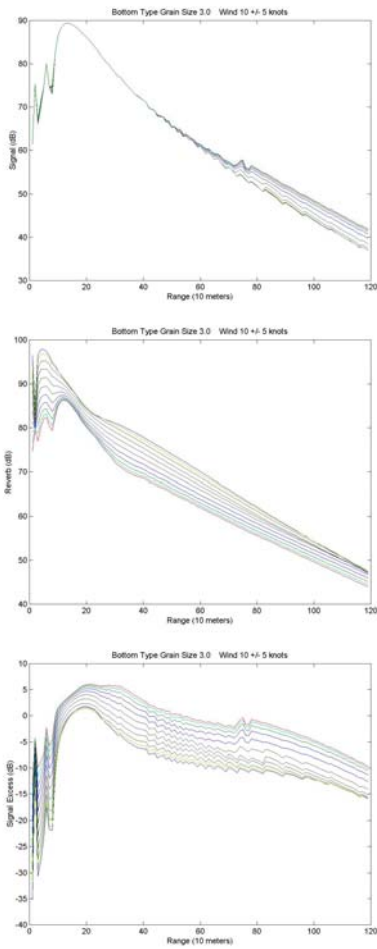


Fig. 10. Range dependent effect of wind variability on acoustic detection for muddy sand at the sea bottom simulated using CASS/GRAB: (a) signal, (b) reverberation, and (c) signal excess.

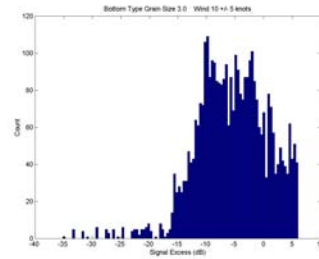


Fig. 11. Histogram of CASS/GRAB simulated signal excess at the sea bottom for muddy sand with surface wind speed varying between 2.5 to 7.5 m/s.

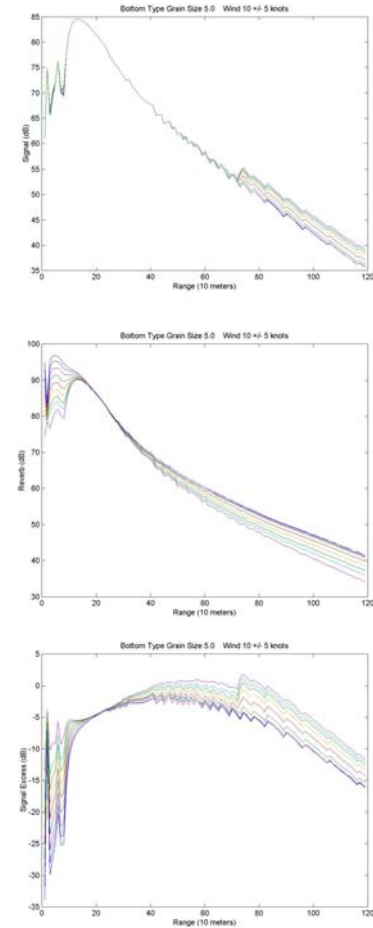


Fig. 12. Range dependent effect of wind variability on acoustic detection for sand silt at the sea bottom simulated using CASS/GRAB: (a) signal, (b) reverberation, and (c) signal excess.

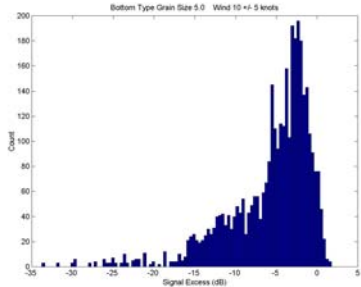


Fig. 13. Histogram of CASS/GRAB simulated signal excess at the sea bottom for sand silt with surface wind speed varying between 2.5 to 7.5 m/s.

5. Acoustic Uncertainty Due to Combined Input Variability

Let the transducer be placed at 5.18 m (17 ft) with a downward tilt angle varying from +4° to -12° in a shelf sea (water depth of 30 m). The range for identifying the acoustic detection at the sea bottom is from 300 m to 1200 m. The bottom type index changes from 0.5 (coarse sand) to 6.0 (silt) with 0.5 increments. The wind variability is taken as 2.5 m/s to 12.5 m/s (5 kts to 25 kts).

Investigating the signal excess at 300 m there are some interesting features to note (Fig. 14). There is a dip in signal excess at bottom type grain size index 5.0 (sandy silt) for all wind speeds and tilt angles down to -8°. For coarse sand to clayey sand, tilt angle -4° presents the highest signal excess for all wind speeds. For tilt angles -4° and down, the finer bottom types, sandy silt to silt, exhibit little sensitivity to wind speed with only a 3 dB difference. Also, for bottom type grain size indexes 4.0 (clayey sand) to silt, tilt angles -4° and down offers higher signal excess for all wind speeds. The signal excess also experiences an elevated value for the highest wind speeds at these fine bottom types for tilt angles -8° and -12°. Wind speed has the greatest effect on muddy gravel to clayey sand for all tilt angles with a peak difference of 14 dB. The highest wind speeds, 20 and 25 kts, display comparable signal excess for all tilt angles and bottom types.

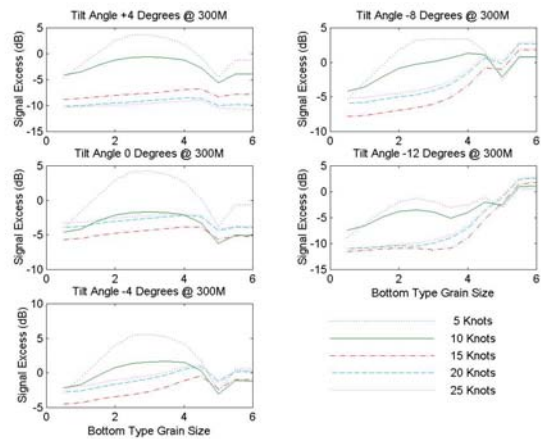


Fig. 14. Dependence of signal excess on bottom grain size index for various tilt angles for shallow transducer (depth: 5.17 m) at range of 300 m: (a) 4°, (b) 0°, (c) -4°, (d) -8°, and (e) -12°. Here five curves in each panel represent different surface wind speed.

The character of the signal excess curves changes at 600 m (Fig. 15). The finer bottom types, sandy silt to silt still exhibit little sensitivity to wind speed for tilt angles -4° and down. However, the peak signal excess values are all shifted to the finer bottom types. The greatest sensitivity to wind speed variation exists for medium bottom types, muddy gravel to clayey sand, at tilt angles of 0° and to a lesser degree for all other tilt angles. The coarse bottom types, coarse sand to muddy gravel, demonstrate maximum signal excess at tilt angle 0°. Wind speeds of 20 and 25 kts continue to display comparable signal excess for all tilt angles and bottom types.

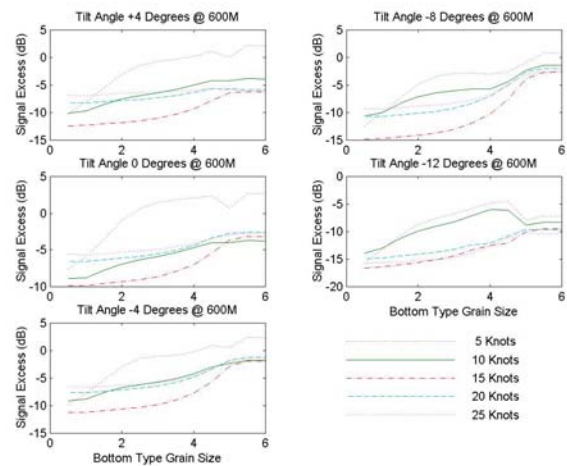


Fig. 15. Same as Fig. 14 except for range of 600 m.

The character of the signal excess curves changes again at 900 m (Fig. 16). For tilt angles down to -4°, the signal excess builds to a maximum for finer bottom types. A tilt angle of 0° offers the best signal excess for all bottom types

and wind speeds, slightly better than -4° tilt angles. For tilt angles -8° and -12° , the signal excess diminishes for the fine bottom types, after building to a peak for medium bottom types. The greatest signal excess variations occur for tilt angle -12° for the medium bottom types, with a peak value of 14 dB difference for very fine sand. Tilt angle -12° offers the lowest signal excess for all wind speeds and bottom types. Wind speeds of 20 and 25 kts show little variation for bottom type or tilt angle and maintain similar values of signal excess.

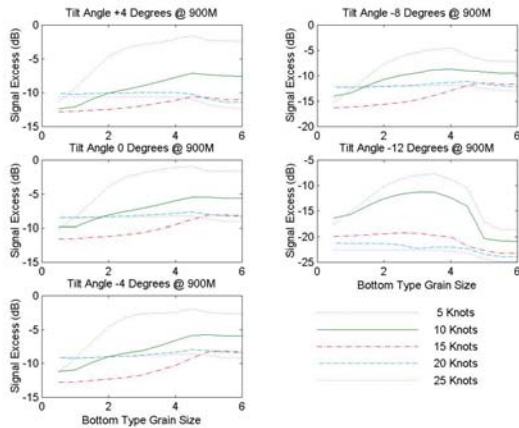


Fig. 16. Same as Fig. 14 except for range of 900 m.

The character of the signal excess curves does not change much from 900 m (Fig. 16) to 1200 m (Fig. 17). Tilt angle of 0° still offers the best signal excess for all bottom types and wind speeds. Tilt angle of -12° contains the greatest signal excess variation of 20 dB for medium bottom types and the lowest signal excess for all bottom types and wind speeds. For tilt angles down to -4° , each wind speed shows little variation in signal excess magnitude from muddy gravel to silt. The histograms of reverberation, signal, and signal excess are for all ranges up to 1200 m, tilt angles $+4^\circ$ to -12° , bottom types gravelly sand to silt, wind speeds 5 to 25 kts, water depth 30 m and transducer depth 5.18 m (Fig. 18). The peak of signal excess is at -7 dB, with a few instances of readings as high as $+7$ dB. The signal excess histogram demonstrates a nearly Gaussian distribution with a left skewed shape due to the farthest ranges and tilt angles of -12° effects. The signal histogram exhibits a bimodal distribution, centered at about 48 and 75 dB with slight left and right skewness. The reverberation histogram also appears to have a slight bimodal distribution, centered at about 50 and 78 dB, nearly matching the signal histogram modes.

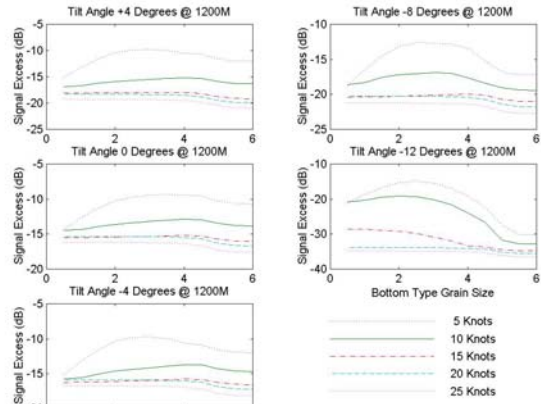


Fig. 17. Same as Fig. 14 except for range of 1200 m.

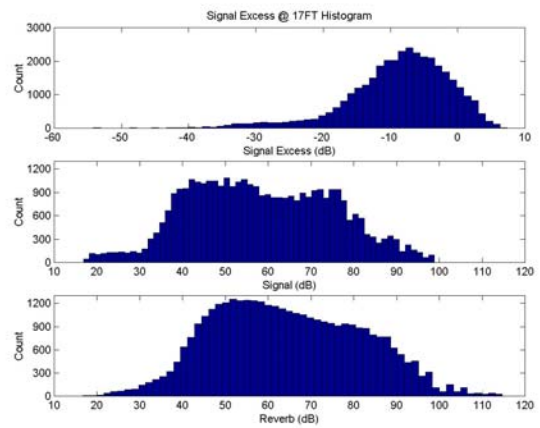


Fig. 18. Histogram of CASS/GRAB simulated signal excess, signal, and reverberation at the sea bottom from a shallow transducer (depth: 5.17 m) with combined input uncertainty.

6. Conclusions

(1) For shallow transducer (depth at 5.18 m), the uncertainty of signal excess for ranges less than 800 m is approximately 3 dB for the muddy sand and 5 dB for the sandy silt; however, for ranges greater than 800 m, the sandy silt is less variable than muddy sandy. For ranges at the peak signal excess, the uncertainty of signal excess reaches a maximum value of 6 dB for the sandy silt that makes the difference between detection and no detection. The importance of this finding is that for this type of bottom target detection, the model may predict an identifiable object; while the actual environment would yield no positive signal excess and hence no detections. This worst case scenario indicates that bottom type data is more significant for acoustic detection. For the present conditions, the muddy sand variability has a small effect on detection since there is a positive signal excess for all cases.

Therefore, for small variations of muddy sand, the impact on detection is minimal.

(2) Employment of a better sensor, if available, would offset the sandy silt variability effect due to inadequate data. Evaluation of these signal excess graphs reveals that a better sensor with 1 to 4 dB gain significantly boosts detection ranges and probability, in spite of the greater variability present. This is due to the fact that sandy silt has a lower signal excess slope than muddy sand with range up to 800 m.

(3) The acoustic uncertainty due to the wind variability is more sensitive to muddy sand than to and sandy silt. Maximum acoustic uncertainty due to wind variability is 9 dB for the muddy sand and 6 dB for the sandy silt. For the bottom target detection, the wind speed accuracy is extremely important. If wind speed uncertainty exceeds 7 kts, the bottom target is unlikely to be detected.

(4) The generic VHF forward looking sonar performance for muddy sand is satisfactory; however, sandy silt requires greater bottom type and wind speed accuracy to determine if detections are likely. In the event higher accuracy bottom type and wind speed data are unattainable for sandy silt bottom types, alternative sensors or tactics are recommended to overcome this sensors shortcomings. The findings indicate that improved sensor performance of a few dB far out weigh the benefits of higher accuracy bottom and wind data. Higher accuracy inputs and improved sensors are expensive, as such; money would be better spent on sensor improvements for a greater return on investment.

(5) The medium bottom types are the most sensitive to wind speed variations for the tilt angles and transducer depths examined. Variations up to 15 dB are demonstrated for wind speed variations of 10 ± 5 kts. Medium bottom types demonstrate greater signal excess at ranges under 300 m, while fine bottom types peak at farther ranges.

(6) At ranges greater than 600 m, tilt angles of -12° provide insufficient signal excess to be useful. The highest wind speeds of 20 and 25 kts have nearly the same signal excess for all tilt angles and bottom types at transducer depth 5.18 m. Transducers at 25 m exhibit the same characteristics with a few exceptions at tilt angle -12° at 600 m and closer.

(7) For bottom target detection, deep transducer (depth: 25 m) demonstrates substantial signal excesses up to 23 dB compared to 7 dB for shallow transducer (depth: 5.18 m). Therefore, to increase the probability of bottom target detection utilizing the generic VHF forward looking sonar, placement of the transducer deeper in the water column is recommended.

References

Chen, C. T. and Millero, F. J., Speed of Sound in Seawater at High Pressures. *Journal of Acoustic Society of America*, **62** (5), 1129-1135, 1977.

Chu, P.C., C.J. Cintron, S.D. Haeger, D. Schneider, R.E. Keenan, and D.N. Fox, Yellow Sea acoustic uncertainty caused by hydrographic data errors. In "*Impact of Littoral Environment Variability on Acoustic Prediction and Sonar Performance*", edited by N.G. Pace and F. B. Jensen. Kluwar Academic Publisher, Boston, 563-570, 2002.

Chu, P.C., N.A. Vares, S.D. Haeger, and R.E. Keenan, Uncertainty in shallow sea acoustic detection due to environmental variability. *Journal of Undersea Acoustics*, 2003, submitted.

Keenan, R. E., An Introduction to GRAB Eigenrays and CASS Reverberation and Signal Excess. *Science Applications International Corporation*, MA, 2000.

Leroy, C. C., Development of Simple Equations for Accurate and More Realistic Calculation of the Sound Speed in Sea Water. *Journal of Acoustic Society of America*, 46 (1), 216-226, 1969.

Millero, F.J. and Li, X., Comments on "On Equations for the Speed of Sound in Seawater". *Journal of Acoustic Society of America*, **95** (5), 2757-2759, 1994.

Naval Oceanographic Office Systems Integration Division, Software Design Document for the Gaussian Ray Bundle (GRAB) Eigenray Propagation Model. *OAML-SDD-74*, Stennis Space Center, MS, 1999.

Naval Oceanographic Office Systems Integration Division, Software Requirements Specification for the Gaussian Ray Bundle (GRAB) Eigenray Propagation Model. *OAML-SRS-74*. Stennis Space Center, MS, 1999.

Weinberg, H., and R. Keenan, Gaussian ray bundles for modeling high-frequency propagation loss under shallow water condition. *Journal of Acoustic Society of America*, **100** (3), 1421-1431, 1996.

Weinberg, H., CASS Roots. *Integrated Performance Decisions*, CT, 2000.